Chromosome missegregation causes somatic polyploidization in plants

Elena Kozgunova[1*], Momoko Nishina[2], Gohta Goshima[2*]

[1]International Collaborative Programme in Science, Graduate School of Science, Nagoya University, Furo-cho, Chikusa-ku, Nagoya, Aichi 464-8602, Japan
[2]Division of Biological Science, Graduate School of Science, Nagoya University, Furo-cho, Chikusa-ku, Nagoya, Aichi 464-8602, Japan
[*]Correspondence should be addressed to kozgunova@gmail.com; goshima@bio.nagoya-u.ac.jp

Polyploidy, or genome multiplication, is common in plants and greatly impacts evolution and speciation. It is generally considered that genome duplication in plants mainly arises through sexual reproduction via unreduced gamete fusion. On the contrary, polyploidization in somatic cells occurs in the differentiated tissues; thus, it is not inherited. In this study, we show that chromosome missegregation during somatic cell division frequently induces polyploidization in the moss *Physcomitrella patens*. We carried out a comprehensive characterization of kinetochore components in moss and found that kinetochore malfunction induces lagging chromosomes, which inhibit the assembly of cytokinetic machinery. The resultant cells were polyploid, proceeded to the next cell cycle, and eventually developed into polyploid plants. We also showed that bi-nucleated *Arabidopsis* embryos that were generated by artificial inhibition of cytokinesis were able to execute the next round of cell division, suggesting that mitotic errors could potentially lead to inheritable polyploidization in diverse plant species.

Introduction

The kinetochore is a macromolecular complex that connects chromosomes to spindle microtubules and plays a central role in chromosome segregation. Kinetochore malfunction causes checkpoint-dependent mitotic arrest, apoptosis, and/or aneuploidy-inducing chromosome missegregation (1). Most of our knowledge on kinetochore function and impact on the genome stability is derived from animal and yeast studies (2). Another major group of eukaryotes, plants, also possesses conserved kinetochore proteins (3–5). Although the localization and loss-of-function phenotype of some plant kinetochore proteins have been reported before (6–15), the data are mostly obtained from fixed cells of specific tissues. No comprehensive picture of plant kinetochore protein dynamics and functions can be drawn as of yet. For example, plants appear to have lost 12 out of 16 components that form CCAN (constitutive centromere associated network) in animal and yeast cells (2, 5), yet how residual CCAN subunits act in plants is unknown.

The moss *Physcomitrella patens* is an emerging model system for plant cell biology. The majority of its tissues are in a haploid state, and, owing to an extremely high rate of homologous recombination, gene disruption and fluorescent protein tagging of endogenous genes are easy to obtain in the first generation (16). Another remarkable feature is its regeneration ability; for example, differentiated gametophore leaf cells, when excised, are efficiently reprogrammed to become stem cells (17, 18). Thus, genome alteration (mutation, polyploidy), even in a somatic cell, can potentially spread through the population.

In this study, we aimed to comprehensively characterize conserved kinetochore proteins in a single plant cell type, the *P. patens* caulonemal apical cell. Unexpectedly, we observed that most of the kinetochore proteins displayed localization patterns distinct from their animal counterparts. Furthermore, kinetochore malfunction resulted in chromosome missegregation and polyploidy via perturbing the function of the cytokinetic machinery.

Results

Endogenous localization analysis of conserved kinetochore proteins in *P. patens*

To observe the endogenous localization of putative kinetochore components, we inserted a fluorescent tag in-frame at the C- or N-terminus of eighteen selected proteins (Fig. S1). Histone H3-like CENP-A (CenH3) localization was determined by ectopic Citrine-CENP-A expression, as tagging likely perturbs its function. Consistent with their sequence homology, many of the proteins were localized to the kinetochore at least transiently during the cell cycle. However, many proteins also showed unexpected localization (or disappearance) at certain cell cycle stages (Fig. 1; Fig. S2–S7; Movies S1-S3). Most surprising were CCAN protein dynamics: CENP-X, CENP-O and CENP-S did not show kinetochore enrichment at any stages (Fig. 1; Fig. S3; Movie S1), whereas CENP-C also dissociated from the kinetochore transiently in the post-mitotic phase (Fig. S4; Movie S2). Thus, we could not identify any "constitutive" kinetochore proteins other than CENP-A.

Kinetochore malfunction causes chromosome missegregation and cytokinesis failure

We failed to obtain knockout lines for all the targeted kinetochore proteins, except for the spindle checkpoint protein Mad2, strongly suggesting that they are essential for moss viability. We therefore selected conditional RNAi lines for functional analyses. In this RNAi system, knockdown of target genes was induced by the addition of β-estradiol to the culture medium 4–6 days prior to live-imaging (19). We first targeted CENP-A, the only constitutive centromeric protein identified in *P. patens*. Since RNAi sometimes exhibits an off-target effect, we prepared two independent RNAi constructs. As expected, we observed a significant mitotic delay and chromosome alignment/segregation defects in the CENP-A RNAi lines (Fig. S8; Movie S4). These phenotypes can be explained by a deficiency in proper kinetochore-microtubule attachment. Consequently, micronuclei were observed in the daughter cells, a hallmark of aneuploidy. We concluded that CENP-A, like in many organisms, is essential for equal chromosome segregation during mitosis in moss.

Surprisingly, we also observed cells with two large nuclei in both RNAi lines (Fig. 2B, 1 h 18 min), which is the typical outcome of cytokinesis failure in this cell type (20–22). To check if a similar phenotype is observed after the depletion of another kinetochore protein, we made conditional RNAi line for SKA1 (the localization of SKA1-Citrine is shown on Fig. S6D, Movie S3), an outermost kinetochore component that does not directly interact with CENP-A. As expected, mitotic delay and chromosome missegregation were observed in the RNAi line (Fig. S8; Movie S4). In addition, cytokinesis failure was also detected (Fig. 2B; Movie S5). To verify that the observed phenotype of SKA1 was not due to an off-target effect, we ectopically expressed RNAi-insensitive SKA1-Cerulean in the RNAi line and observed the rescue of all the above phenotypes (Fig. S9).

Although we could not detect any kinetochore enrichment of the CCAN subunit CENP-X, we analyzed its RNAi lines. Interestingly, we observed similar phenotypes to CENP-A and SKA1, including cytokinesis failure (Fig. 2B; Fig. S8; Movie S4). CENP-X RNAi phenotypes were rescued by the ectopic expression of CENP-X-Cerulean that was resistant to the RNAi

construct (Fig. S9). Thus, CENP-X has lost its kinetochore localization in moss, but is still essential for chromosome segregation and cell division.

During plant cytokinesis, a bipolar microtubule-based structure known as the phragmoplast is assembled between segregating chromatids. The cell plate then forms in the phragmoplast midzone (~4 min after anaphase onset in *P. patens* caulonemal cells) and gradually expands towards the cell cortex, guided by the phragmoplast (20). We observed that microtubules reorganized into phragmoplast-like structures upon chromosome segregation in every cell, regardless of the severity of chromosome missegregation (e.g. 32 min in Fig. 2B). However, by analyzing a total of 44 cells from SKA1 (9 cells), CENP-X (18 cells) and CENP-A RNAi (9 cells for one construct and 8 cells for the other) lines that had lagging chromosomes, we noticed a correlation between cytokinesis failure and lagging chromosomes lingering for a relatively long time in the space between separated chromatids. We therefore quantified the duration of lagging chromosomes' residence in the midzone between separating chromatids following anaphase onset. Interestingly, a minor delay of chromosomes in the midzone (< 4 min) never perturbed cytokinesis (100%, n = 9 for CENP-A, n = 4 for CENP-X and n = 3 for SKA1). By contrast, if we observed a longer delay of chromosome clearance from the midzone, even when only a single chromosome was detectable, cytokinesis defects occurred in 96% of the cells (n = 9, 14 and 5; Fig. 2C, D). Next, we checked if the cell plate was formed at any point in the cells that had cytokinesis defects, using the lipophilic FM4-64 dye. We could not observe vesicle fusion at the midzone following anaphase onset; thus, the cell plate did not form in the cells that had lagging chromosomes for a long time (Movie S6). From these results, we concluded that occupation of the midzone by lagging chromosomes for several minutes prevents cell plate formation, which subsequently causes cytokinesis failure.

Polyploid plants are regenerated from isolated multi-nucleated cells.

Lagging chromosomes are a major cause of aneuploidy in daughter cells, which is particularly deleterious for haploid cells. However, the above observation supports a different scenario, whereby cytokinesis failure induced by lagging chromosomes allows a cell to have a duplicated genome set in two or more nuclei. On the other hand, whether animal somatic cells that have failed cytokinesis can re-enter the cell cycle or not remains an ongoing debate (23–25). To address whether moss cells can recover from severe cell division defects and continue their cell cycle, we first analyzed the DNA content of cells in the CENP-A exon-targeting RNAi line, in which multi-nucleated cells were most prevalent. For comparison, we used the parental line: the nuclei of anaphase/telophase cells served as the 1N reference and randomly selected interphase nuclei as the 2N reference, as caulonemal cells are mostly in the G2 phase (18, 26). We observed that the majority of the multi-nucleated cells after CENP-A RNAi underwent DNA replication and became tetraploid or attained even higher ploidy (Fig. 3A; DNA was quantified at day 5 after β-estradiol treatment).

Next, we checked if multi-nucleated cells continue cell cycling. We used SKA1 RNAi line for a long (46 h) time-lapse imaging; with this imaging, we expected to monitor a process of cytokinesis failure of a haploid cell and its fate. During the imaging period, we indeed observed cytokinesis failure and 10% or 25% multi-nucleated apical cells executed next cell division by forming a single spindle (n = 43 and 25 for experiments 1 and 2, respectively, Fig. 3B; Movie S7). This data strongly suggests that cells that have undergone cytokinesis failure can continue cell cycling as diploids at a certain probability.

Diploid *P. patens* is known to develop protonema tissue but hardly any gametophores (leafy shoots) (27); therefore, it was expected that a multi-nucleated cell

produced by cytokinesis failure of a caulonemal cell would proliferate and form a large protonema colony. To verify this, we isolated and cultured several cells (Fig. 3C) that were seemingly multi-nuclear after SKA1 RNAi via laser dissection microscopy (note that there is an unambiguity in identifying multi-nucleate cells; see Methods for detailed explanation). After 6 weeks of culturing without β-estradiol, we obtained four moss colonies, two of which consisted mainly of protonemal cells (Fig. 3D, colony 3 and 4). DNA staining and quantification showed that the majority of the cells derived from those two colonies had DNA content approximately double of the control haploid cells, which were regenerated in an identical manner (Fig. 3E, colony 3 and 4, regenerated from cell 3 and 4, respectively). Thus, it was confirmed that a polyploid plant can be regenerated from a single multi-nucleated somatic cell.

Consequence of cytokinesis failure in the *Arabidopsis* embryo

Genome duplication that occurs in somatic cells of angiosperms can only lead to an organism with mixed ploidy, and the duplicated state is rarely passed on to the gametes. In addition, multiple factors limit the formation of polyploid zygotes through sexual reproduction, such as the low frequency of unreduced gamete formation/fusion or the "triploid block" of the endosperm (28). However, if the cytokinesis failure and subsequent cell cycling occur during early embryo development, it can give rise to an organism in which most, if not all, cells have a duplicated genome, leading to an inheritable increase in ploidy. To test this possibility, we artificially induced cytokinesis failure in the first division of *A. thaliana* embryos by treatment with the microtubule-depolymerizing drug oryzalin and observed the resulting bi-nucleated cell following oryzalin washout (Fig. 3F; Movie S8). Notably, all three bi-nucleated embryos we observed re-entered the mitotic phase, as characterized by chromosome condensation. Taking into consideration that polyploid *Arabidopsis* species are found in nature (29), we suggest that tetraploid embryos formed due to mitotic errors can continue their development and produce a whole plant at a certain probability. It is worth mentioning that microtubule-depolymerizing drugs, such as colchicine, have been used for decades to produce polyploid plants (30), yet little is known about the mechanism underlying polyploid induction. Unlike this study, previous studies observed the effects of microtubule-depolymerizing drugs applied to the whole plant over a long period of time and proposed that polyploidization is caused by endoreduplication, rather than cytokinesis failure (31).

Discussion

Kinetochore protein dynamics in a plant cell

This study provides a comprehensive view of the dynamics of conserved kinetochore proteins in a single cell type of *P. patens*; furthermore, several proteins, including borealin, KNL1 and SKA subunits, have been characterized for the first time in plant cells. Overall, the behavior of outer subunits was largely consistent with their animal counterparts, suggesting that the mitotic function is also conserved. However, the timing of kinetochore enrichment differed from that of animal cells and even flowering plants (e.g. Arabidopsis, maize) (6, 14, 32): for example, *P. patens* Ndc80 complex gradually accumulated at the kinetochore after NEBD, unlike Arabidopsis and maize, where it showed kinetochore enrichment throughout the cell cycle (6, 14). In contrast, more unexpected localizations were observed for inner CCAN subunits, namely CENP-C, CENP-O, CENP-S and CENP-X. For example, CENP-C disappeared from the centromeres shortly after mitotic exit. In animal cells, CENP-C has been suggested to act in cooperation with Mis18BP1/KNL2 to facilitate CENP-A deposition in late telophase and early G1 (2). Hence, the mechanism of CENP-A incorporation might have been modified in plants.

CENP-O, -S, or –X did not show kinetochore enrichment at any stage. CENP-X localization was unlikely an artifact of Citrine tagging, since the tagged protein rescued the RNAi phenotype. In human cells, sixteen CCAN subunits, forming four sub-complexes, have been identified and shown to be critical for kinetochore assembly and function, not only in cells, but also in reconstitution systems (33, 34). In plants, only four CCAN homologues have been identified through sequence homology search. It is therefore possible that less conserved CCAN subunits are present, but could not be identified by the homology search. However, the complete lack of kinetochore localization for CENP-O, -S, -X suggests that plants have lost the entire kinetochore-enriched CCAN complex. Somewhat puzzlingly, CENP-X, despite its unusual localization, remained an essential factor for chromosome segregation in *P. patens*. In animals, it has been proposed that CENP-S and CENP-X form a complex and play an important in outer kinetochore assembly (35). It is an interesting target for further investigation if plant CENP-S/CENP-X preserves such a function.

Chromosome missegregation causes polyploidization

We observed lagging chromosomes as well as cytokinesis failure after knocking down kinetochore components. Failure in chromosome separation/segregation and cytokinesis can be caused by a single gene mutation, if the gene has multiple functions; for example, separase Rsw4 (*radially swollen4*) in *A. thaliana* is involved in sister chromatid separation, Cyclin B turnover and vesicle trafficking that is required for phragmoplast formation (36–39). By contrast, in our study, both phenotypes were observed after RNAi treatment of CENP-A, a constitutive centromeric histone protein that is unlikely to play a direct role in cytokinesis. Furthermore, the cytokinesis phenotype also appeared in CENP-X and SKA1 RNAi lines, and only when lagging chromosomes persisted for several minutes or longer. Based on these data, we propose that persistent lagging chromosomes cause cytokinesis failure. Lagging chromosomes might act as physical obstacles to perturb phragmoplast microtubule amplification and/or cell plate formation. Alternatively, lagging chromosomes might produce a signal that inhibits phragmoplast expansion or cell plate formation in order to prevent chromosome damage, reminiscent of the NoCut pathway in animal cytokinesis (40, 41).

Our data further suggest that in *P. patens*, chromosome missegregation in a single cell could lead to the generation of polyploid plants. This proposal is based on three lines of data. First, we confirmed higher ploidy of the multi-nucleated cells based on DNA quantity measurement (Fig. 3A). Second, we observed that cytokinesis-failed cells re-entered the mitotic phase, indicating continuous cell cycling (Fig. 3B). The reason for the low frequency of this event (~15%) is unclear; strong chromosome missegregation might result in a severe "aneuploid" state for each nucleus, whereas the cell is overall polyploid, which might change the cell physiology. Finally, we isolated single cells that experienced cytokinesis failure and observed the development of the polyploid protonemal tissue (Fig. 3C–E).

Could lagging chromosomes cause polyploidization through somatic cell lineage in wild-type plants? In our imaging of control moss cells, we could not find any lagging chromosome, since mitotic fidelity is very high in our culture conditions. Intriguingly, however, lagging chromosomes (or "chromosome bridges") have been long observed in wild-type plants and crops, albeit at a low frequency. For example, McClintock (1938) described abnormal anaphase and telophase behavior of ring chromosomes in 0.16 to 8% of root cells in maize (42). Various abnormalities in mitosis and chromosome aberrations were detected in 21% of the leaf cells of *Coffea arabica* (43), and in 1.6 to 13 % of the leaf cells of different varieties of *Allium* (44), *Scots pine*, *Siberian fir* and other species (45). Furthermore,

various hybrid plants exhibit lagging chromosomes, anaphase bridges and cytokinesis abnormalities in meiosis (46, 47). To the best of our knowledge, those studies never analyzed the relationship between lagging chromosomes and cytokinesis integrity; we expect the presence of lagging chromosomes for a certain duration to similarly perturb cytokinesis as observed in our study of moss, since the cytokinesis process is highly conserved between bryophytes and angiosperms (48). Genome sequencing suggests that *P. patens*, like many other plant species, experienced whole genome duplication at least once during evolution (49). Polyploidization through spontaneous mitotic errors in somatic cells might have a greater impact on *de novo* formation of polyploid plants than previously anticipated.

Materials and Methods

Moss culture and transformation

We generally followed protocols described by Yamada *et al* (50). In brief, *Physcomitrella patens* culture was maintained on BCDAT medium at 25°C under continuous light. Transformation was performed with the polyethylene glycol-mediated method and successful endogenous tagging of the selected genes was confirmed by PCR (50). We used *P. patens* expressing mCherry-α-tubulin under the pEF1α promoter as a host line, except for Mis12-mCherry line where GFP-α-tubulin line was used as a host line. For knockout, CRISPR (51) and RNAi transformations, we used the GH line, expressing GFP-tubulin and HistoneH2B-mRFP. *P. patens* lines developed for this study are described in Dataset S1.

Plasmid construction

Plasmids and primers used in this study are listed in Dataset S2. For the C-terminal tagging we constructed integration plasmids, in which ~800 bp C-terminus and ~800 bp 3'-UTR sequence of the kinetochore gene were flanking the *citrine* gene, the nopaline synthase polyadenylation signal (nos-ter), and the G418 resistance cassette. For the N-terminal tagging we constructed integration plasmids, in which ~800 bp 5'-UTR and ~800 bp N-terminus sequence of the kinetochore gene were flanking the *citrine* gene. CENP-A cDNA was amplified by PCR and sub-cloned into a vector containing the rice actin promoter, *citrine* gene, the rbcS terminator, the modified *aph4* cassette, and flanked by the genomic fragment of the *hb7* locus to facilitate integration. All plasmids were assembled with the In-Fusion enzyme according to manufacturer's protocol (Clontech). RNAi constructs were made by using the Gateway system (Invitrogen) with pGG624 as the destination vector (52).

DNA staining

We followed the protocol described by Vidali *et al* (53) with the following modifications: sonicated moss was cultured for 6–7 days on the BCDAT plate, containing 5 μM β-estradiol for RNAi induction and 20 μg/ml G418 to prevent contamination. Collected cells were preserved in fixative solution (2% formaldehyde, 25 mM PIPES, pH 6.8, 5 mM $MgCl_2$, 1 mM $CaCl_2$) for 30 min and washed three times with PME buffer (25 mM PIPES, pH 6.8, 5 mM $MgCl_2$, 5 mM EGTA). Following fixation, cells were mounted on 0.1% PEI (polyethyleneimine)-coated glass slides and subsequently incubated with 0.1% Triton X-100 in PME for 30 min and 0.2% driselase (Sigma-Aldrich) in PME for 30 min. Next, cells were washed twice in PME, twice in TBS-T buffer (125 mM NaCl, 25 mM Tris-HCl, pH 8, and 0.05% Tween 20) and mounted in 10 μg/mL DAPI in TBS-T for observation. Images were acquired with the Olympus BX-51 fluorescence microscope equipped with ZEISS Axiocam 506 Color and controlled by ZEN software. Fluorescent intensity was measured with ImageJ. Cytoplasmic background was subtracted.

Live-imaging microscopy

A glass-bottom dish (Mattek) inoculated with moss was prepared as described in Yamada et

al (50) and incubated at 25°C under continuous light for 4–7 days before live-imaging. To observe RNAi lines, we added 5 μM β-estradiol to culture medium (52). For the high magnification time-lapse microscopy, the Nikon Ti microscope (60×1.40-NA lens) equipped with the spinning-disk confocal unit CSU-X1 (Yokogawa) and an electron-multiplying charge-coupled device camera (ImagEM; Hamamatsu) was used. Images were acquired every 30 s for localization analysis and every 2 min for RNAi analysis. The microscope was controlled by the Micro-Manager software and the data was analyzed with ImageJ. The rescue lines for RNAi and *A. thaliana* embryos were observed using a fluorescence microscope (IX-83; Olympus) equipped with a Nipkow disk confocal unit (CSU-W1; Yokogawa Electric) controlled by Metamorph software. The *A. thaliana* line harboring the embryonic microtubule marker (EC1p::Clover-TUA6) and nuclear marker (ABI4p::H2B-tdTomato) was generated by Kimata *et al* (54).

Single cell isolation

Protonema tissue of *P. patens* was sonicated, diluted with BCD medium with 0.8% agar and spread on cellophane-covered BCDAT plates that contain 5 μM estradiol to induce RNAi. After 5–6 days, small pieces of cellophane with small clusters of protonemal cells (each containing 3–20 cells) were cut with scissors and placed upside-down on the glass-bottom dish. Bi- or multi-nucleated cells were identified using Axio Zoom.v16. Single bi-nucleated cell (Ska1 RNAi line) or random cell (control GH line) was selected for isolation and all other cells were ablated with a solid-state ultraviolet laser (355 nm) through a 20X objective lens (LD Plan-NEOFLUAR, NA 0.40; Zeiss) at a laser focus diameter of less than 1 μm using the laser pressure catapulting function of the PALM microdissection system (Zeiss). Irradiation was targeted to a position distantly located from the cell selected for isolation to minimize the irradiation effect. Note that visual distinction of multi-nucleated cells from those with slightly deformed nuclei is not easy in *P. patens*, since in multi-nucleated cells, the nuclei maintain very close association with each other, so that nuclear boundaries often overlap. We interpret that two of four regenerated protonemata had haploid DNA content due to our unintentional isolation of a single cell with a deformed nucleus rather than multi-nuclei. Next, a piece of cellophane with single isolated cell was transferred from the glass-bottom dish to estradiol-free medium (20 μg/ml G418 was supplied to prevent bacterial/fungal contamination). DAPI staining was performed 5–6 weeks later as described above.

Sequence analysis.

Full-size amino acid sequences of the selected proteins were aligned using MAFFT ver. 7.043 and then revised manually with MacClade ver. 4.08 OSX. We used the Jones-Taylor-Thornton (JTT) model to construct maximum-likelihood trees in MEGA5 software. Statistical support for internal branches by bootstrap analyses was calculated using 1,000 replications. Reference numbers correspond to Phytozome (www.phytozome.net) for *Physcomitrella patens*, the Arabidopsis Information Resource (www.arabidopsis.org) for *Arabidopsis thaliana* and Uniprot (www.uniprot.org) for *Homo sapiens*.

Acknowledgements

We are grateful to Dr. Minako Ueda and Yusuke Kimata for providing *A. thaliana* plants and discussion; to Dr. Yoshikatsu Sato and Nagisa Sugimoto for their assistance with laser ablation experiments; to Dr. Peishan Yi, Moé Yamada and Shu Yao Leong for comments and discussion; Rie Inaba for technical assistance. Imaging was partly conducted in the Institute of Transformative Bio-Molecules (WPI-ITbM) at Nagoya University, supported by Japan Advanced Plant Science Network. This work was funded by JSPS KAKENHI (17H06471, 17H01431) to G.G. The authors declare no competing financial interests.

References

1. Potapova T, Gorbsky G (2017) The Consequences of Chromosome Segregation Errors in Mitosis and Meiosis. *Biology (Basel)* 6(1):12.
2. Musacchio A, Desai A (2017) A Molecular View of Kinetochore Assembly and Function. *Biology (Basel)* 6(5). doi:10.3390/biology6010005.
3. Yu H, Hiatt EN, Dawe RK (2000) The plant kinetochore. *Trends Plant Sci* 5(12):543–547.
4. Hooff JJE Van, Kops GJPL, Tromer E, Wijk LM Van (2017) Evolutionary dynamics of the kinetochore network in eukaryotes as revealed by comparative genomics. *EMBO Rep* 18(9):1559–1571.
5. Yamada M, Goshima G (2017) Mitotic Spindle Assembly in Land Plants: Molecules and Mechanisms. *Biology (Basel)* 6(1):6.
6. Jinwoo Shin, Goowon Jeong, Jong-Yoon Park HK and IL (2018) MUN (MERISTEM UNSTRUCTURED), encoding a SPC24 homolog of NDC80 kinetochore complex, affects development through cell division in Arabidopsis thaliana. *Plant J* 12(10):3218–3221.
7. Zhang H, et al. (2018) Role of the BUB3 protein in phragmoplast microtubule reorganization during cytokinesis. *Nat Plants* 4(July). doi:10.1038/s41477-018-0192-z.
8. Wang M, et al. (2012) BRK1 , a Bub1-Related Kinase , Is Essential for Generating Proper Tension between Homologous Kinetochores at Metaphase I of Rice Meiosis. *Plant Cell* 24(December):4961–4973.
9. Paganelli L, Lecomte P, Deslandes L (2009) Spindle Assembly Checkpoint Protein Dynamics Reveal Conserved and Unsuspected Roles in Plant Cell Division. *PLoS One* 4(8). doi:10.1371/journal.pone.0006757.
10. Komaki S, Schnittger A (2017) The Spindle Assembly Checkpoint in Arabidopsis Is Rapidly Shut Off during Severe Stress. *Dev Cell* 43(2):172–185.e5.
11. Lermontova I, et al. (2013) Arabidopsis KINETOCHORE NULL2 Is an Upstream Component for Centromeric Histone H3 Variant cenH3 Deposition at Centromeres. *Plant Cell* 25(September):3389–3404.
12. Sandmann M, et al. (2017) Targeting of Arabidopsis KNL2 to Centromeres Depends on the Conserved CENPC-k Motif in Its C Terminus. *Plant Cell* 29(January):144–155.
13. Sato H, Shibata F, Murata M (2005) Characterization of a Mis12 homologue in Arabidopsis thaliana. *Chromosom Res* 13(8):827–834.
14. Du Y, Dawe RK (2007) Maize NDC80 is a constitutive feature of the central kinetochore. *Chromosom Res*:767–775.
15. Ogura Y, et al. (2004) Characterization of a CENP-C homolog in Arabidopsis thaliana. *Genes Genet Syst* 79(3):139–144.
16. Cove D, Bezanilla M, Harries P, Quatrano R (2006) Mosses as Model Systems for the Study of Metabolism and Development. *Annu Rev Plant Biol* 57:497–520.
17. Sato Y, et al. (2017) Cells reprogramming to stem cells inhibit the reprogramming of adjacent cells in the moss Physcomitrella patens. *Sci Rep* 7(1):1–12.
18. Ishikawa M, et al. (2011) Physcomitrella Cyclin-Dependent Kinase A Links Cell Cycle Reactivation to Other Cellular Changes during Reprogramming of Leaf Cells C W OA. *Plant Cell* 23(8):2924–2938.
19. Nakaoka Y, et al. (2012) An Inducible

RNA Interference System in Physcomitrella patens Reveals a Dominant Role of Augmin in Phragmoplast Microtubule Generation. *Plant Cell* 24(April):1478–1493.

20. Kosetsu K, Keijzer J De, Janson ME, Goshima G (2013) MICROTUBULE-ASSOCIATED PROTEIN65 Is Essential for Maintenance of Phragmoplast Bipolarity and Formation of the Cell Plate in Physcomitrella patens. *Plant Cell* 25(November):4479–4492.
21. Miki T, Naito H, Nishina M, Goshima G (2014) Endogenous localizome identifies 43 mitotic kinesins in a plant cell. *Proc Natl Acad Sci* 111(11):1053–1061.
22. Naito H, Goshima G (2015) NACK Kinesin Is Required for Metaphase Chromosome Alignment and Cytokinesis in the Moss Physcomitrella Patens. *Cell Struct Funct* 41:31–41.
23. Ganem NJ, Pellman D (2007) Limiting the Proliferation of Polyploid Cells. *Cell* 131(3):437–440.
24. Uetake Y, Sluder G (2004) Cell cycle progression after cleavage failure: Mammalian somatic cells do not possess a “tetraploidy checkpoint.” *J Cell Biol* 165(5):609–615.
25. Panopoulos A, et al. (2014) Failure of cell cleavage induces senescence in tetraploid primary cells. *Mol Biol Cell* 25(20):3105–3118.
26. Schween G, Gorr G, Hohe A, Reski R (2003) Unique tissue-specific cell cycle in Physcomitrella. *Plant Biol* 5(1):50–58.
27. Schween G, Schulte J, Reski R (2005) Effect of Ploidy Level on Growth , Differentiation , and Morphology in Physcomitrella patens *Bryologist* 108(1):27–35.
28. Köhler C, Mittelsten Scheid O, Erilova A (2010) The impact of the triploid block on the origin and evolution of polyploid plants. *Trends Genet* 26(3):142–148.
29. Novikova PY, Hohmann N, Van de Peer Y (2018) Polyploid Arabidopsis species originated around recent glaciation maxima. *Curr Opin Plant Biol* 42:8–15.
30. Hegarty M, et al. (2013) Lessons from natural and artificial polyploids in higher plants. *Cytogenet Genome Res* 140(2–4):204–225.
31. Caperta AD, et al. (2006) Colchicine-induced polyploidization depends on tubulin polymerization in c-metaphase cells. *Protoplasma* 227(2–4):147–153.
32. Hori, T. Tokuko Haraguchi, Yasushi Hiraoka HK and TF (2003) Dynamic behavior of Nuf2-Hec1 complex that localizes to the centrosome and centromere and is essential for mitotic progression in vertebrate cells. *J Cell Sci* 116(16):3347–3362.
33. Guse A, Carroll CW, Moree B, Fuller CJ, Straight AF (2012) In vitro centromere and kinetochore assembly on defined chromatin templates. *Nature* 477(7364):354–358.
34. Weir JR, et al. (2016) Insights from biochemical reconstitution into the architecture of human kinetochores. *Nature* 537(7619):249–253.
35. Amano M, et al. (2009) The CENP-S complex is essential for the stable assembly of outer kinetochore structure. *J Cell Biol* 186(2):173–182.
36. Chang DC, Xu N, Luo KQ (2003) Degradation of cyclin B is required for the onset of anaphase in mammalian cells. *J Biol Chem* 278(39):37865–37873.
37. Yang X, et al. (2011) The radially swollen 4 separase mutation of arabidopsis thaliana blocks chromosome disjunction and disrupts the radial microtubule system in

meiocytes. *PLoS One* 6(4). doi:10.1371/journal.pone.0019459.

38. Moschou PN, et al. (2013) The Caspase-Related Protease Separase (EXTRA SPINDLE POLES) Regulates Cell Polarity and Cytokinesis in Arabidopsis. *Plant Cell* 25(6):2171–2186.
39. Wu S, et al. (2010) A conditional mutation in Arabidopsis thaliana separase induces chromosome non-disjunction, aberrant morphogenesis and cyclin B1;1 stability. *Development* 137:953–961.
40. Norden C, et al. (2006) The NoCut Pathway Links Completion of Cytokinesis to Spindle Midzone Function to Prevent Chromosome Breakage. *Cell* 125(1):85–98.
41. Amaral N, et al. (2016) The Aurora-B-dependent NoCut checkpoint prevents damage of anaphase bridges after DNA replication stress. *Nat Cell Biol* 18(5):516–526.
42. McClintock B (1938) The Production of Homozygous Deficient Tissues with Mutant Characteristics by Means of the Aberrant Mitotic Behavior of Ring-Shaped Chromosomes. *Genetics* 23(4):315–376.
43. Menéndez-Yuffá A, Fernandez-Da Silva R, Rios L, Xena de Enrech N (2000) Mitotic aberrations in coffee (Coffea arabica cv. 'Catimor') leaf explants and their derived embryogenic calli. *Electron J Biotechnol* 3(2):161–166.
44. Nichols C (1941) Spontaneous chromosome aberrations in Allium. *Genetics* 26(1):89–100.
45. Kvitko O V., Muratova EN, Bazhina E V. (2011) Cytogenetics of Abies sibirica in decline fir stands of West Sayan High Mountains. *Contemp Probl Ecol* 4(6):641–646.
46. An H, et al. (2015) Chromosomal behavior during meiosis in the progeny of Triticum timopheevii x hexaploid wild oat. *PLoS One* 10(5):4–5.
47. Matsuoka Y, et al. (2013) Genetic Basis for Spontaneous Hybrid Genome Doubling during Allopolyploid Speciation of Common Wheat Shown by Natural Variation Analyses of the Paternal Species. *PLoS One* 8(8):1–17.
48. Smertenko A, et al. (2017) Plant Cytokinesis: Terminology for Structures and Processes. *Trends Cell Biol* 27(12):885–894.
49. Rensing, et al. (2008) The Physcomitrella Genome Reveals Evolutionary Insights into the Conquest of Land by Plants. *Science (80-)* 319(5859):64–69.
50. Yamada M, Miki T, Goshima G(2016) Imaging Mitosis in the Moss Physcomitrella patens. *Media* 1413:293–326.
51. Lopez-Obando M, et al. (2016) Simple and Efficient Targeting of Multiple Genes Through CRISPR-Cas9 in Physcomitrella patens. *G3 Genes|Genomes|Genetics* 6(November):3647–3653.
52. Miki T, Nakaoka Y, Goshima G (2016) Live Cell Microscopy-Based RNAi Screening in the Moss Physcomitrella patens. *Methods Mol Biol* 1470:225–246.
53. Vidali L, Augustine RC, Kleinman KP, Bezanilla M (2007) Profilin Is Essential for Tip Growth in the Moss Physcomitrella patens. *Plant Cell* 19(11):3705–3722.
54. Kimata Y, et al. (2016) Cytoskeleton dynamics control the first asymmetric cell division in Arabidopsis zygote. *Proc Natl Acad Sci* 113(49):14157–14162.

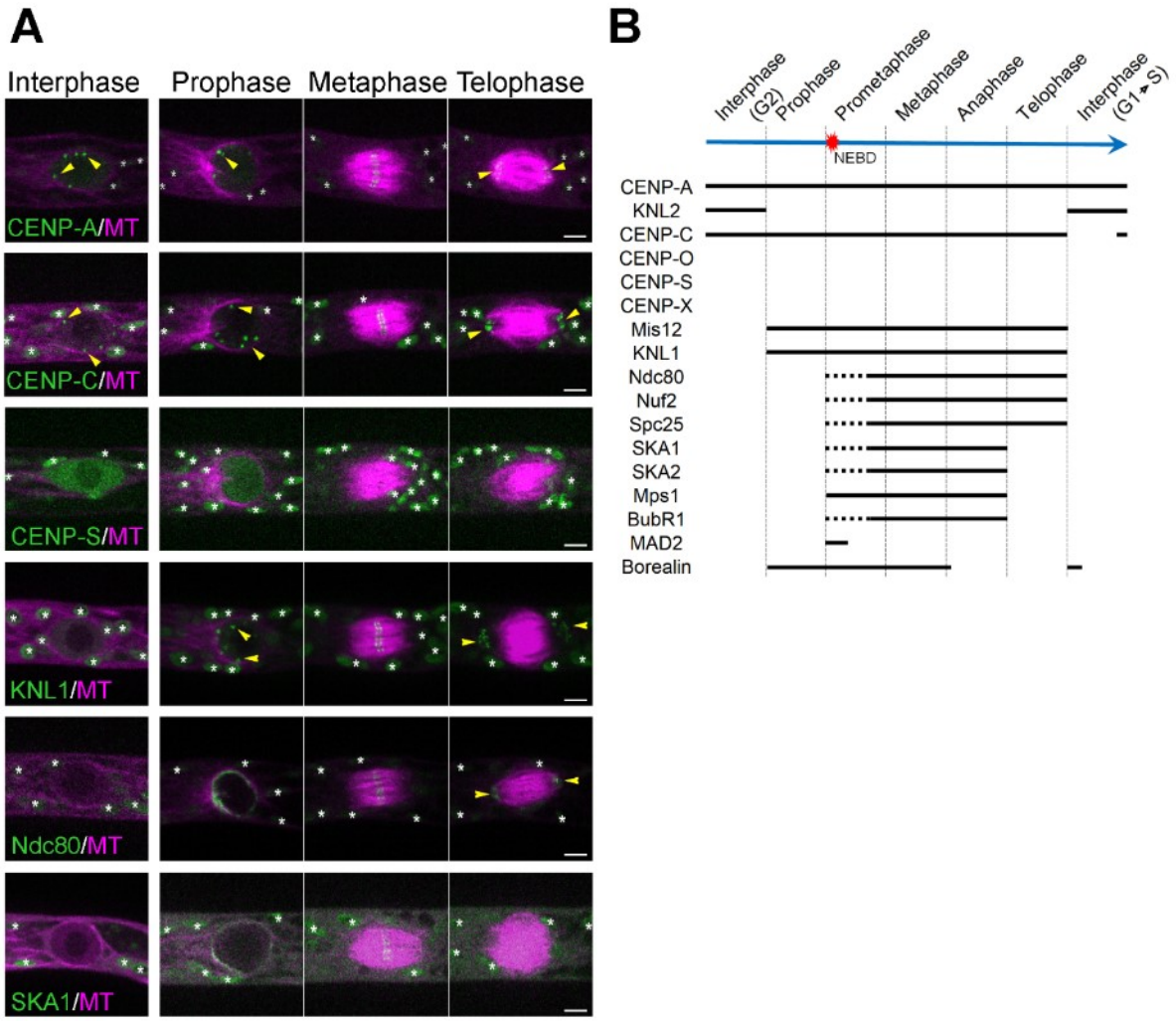

Figure 1. Unconventional localization of kinetochore proteins in *P. patens*.
(A) Live imaging of *P. patens* caulonemal apical cells expressing mCherry-tubulin and selected kinetochore proteins: Citrine-CENP-A; Citrine-CENP-C; Citrine-CENP-S; KNL1-Citrine; Ndc80-Citrine and SKA1-Citrine. Full localization data can be found in Supplemental data. Some kinetochore signals are marked with yellow arrowheads, whereas autofluorescent chloroplasts are all marked with white asterisks. Images were acquired at a single focal plane. Bars, 5 µm. (B) Timeline of kinetochore localization during the cell cycle in *P. patens* caulonemal apical cells. Solid lines correspond to the detection of clear kinetochore signals, whereas dotted lines indicate more disperse signals.

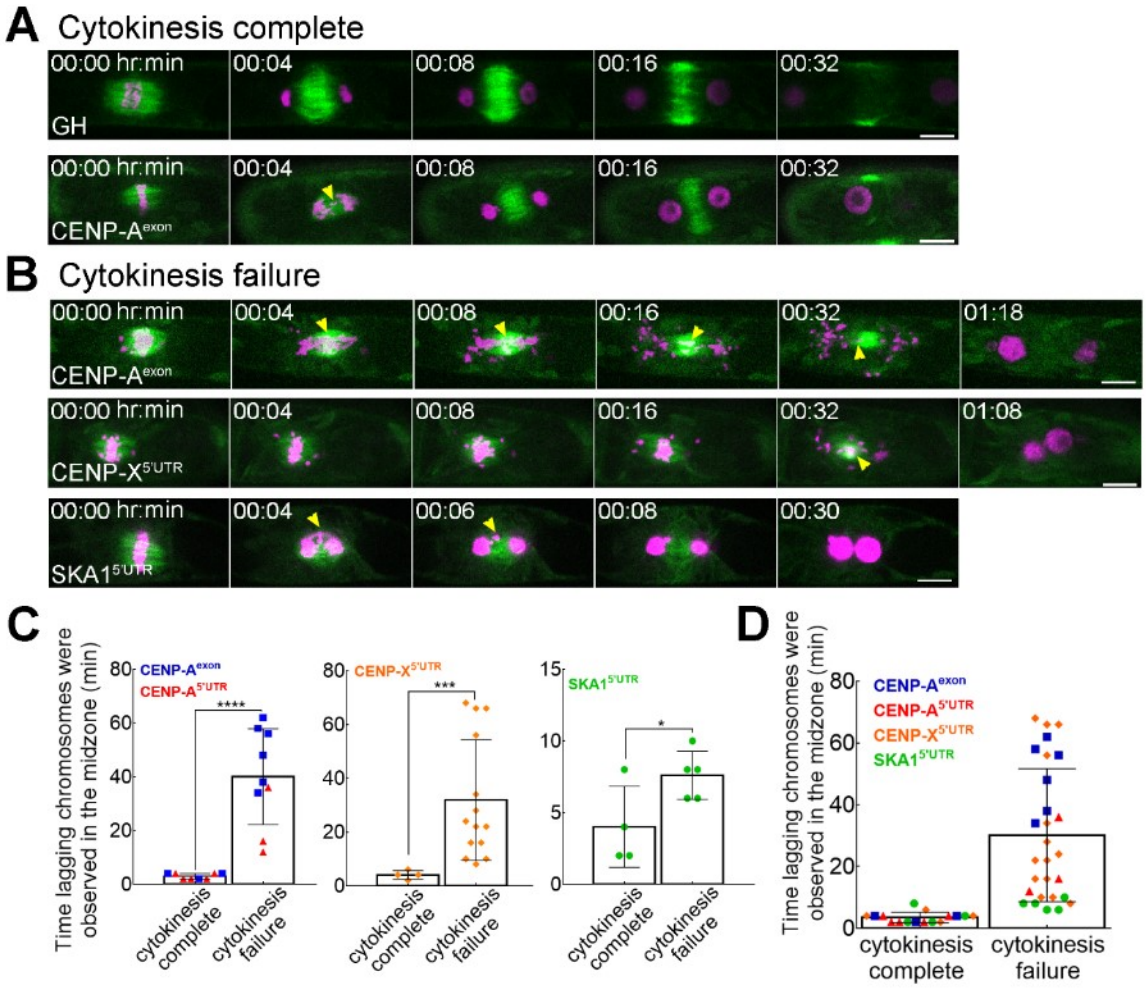

Figure 2. Lagging chromosomes in anaphase induce cytokinesis failure.
(A, B) Lagging chromosomes (yellow arrowheads) present for several minutes in the midzone between separated chromatids cause cytokinesis failure in CENP-A, CENP-X and SKA1 RNAi lines. GH represents a control line. Bars, 10 µm. (C, D) Correlation between cytokinesis failure and duration of lagging chromosomes observed in the midzone in the individual RNAi lines (C) and as combined data (D). Asterisks indicate significant differences between two groups (lagging chromosomes observed for short time or for several minutes) for two outcomes: cytokinesis complete and cytokinesis failure, calculated individually for CENP-A; CENP-X and SKA1 RNAi lines (*P = 0.0476, ***P = 0.0003, ****P < 0.0001; Fisher's test; see Table S1). Each data point corresponds to a single cell. Mean ± SD are presented.

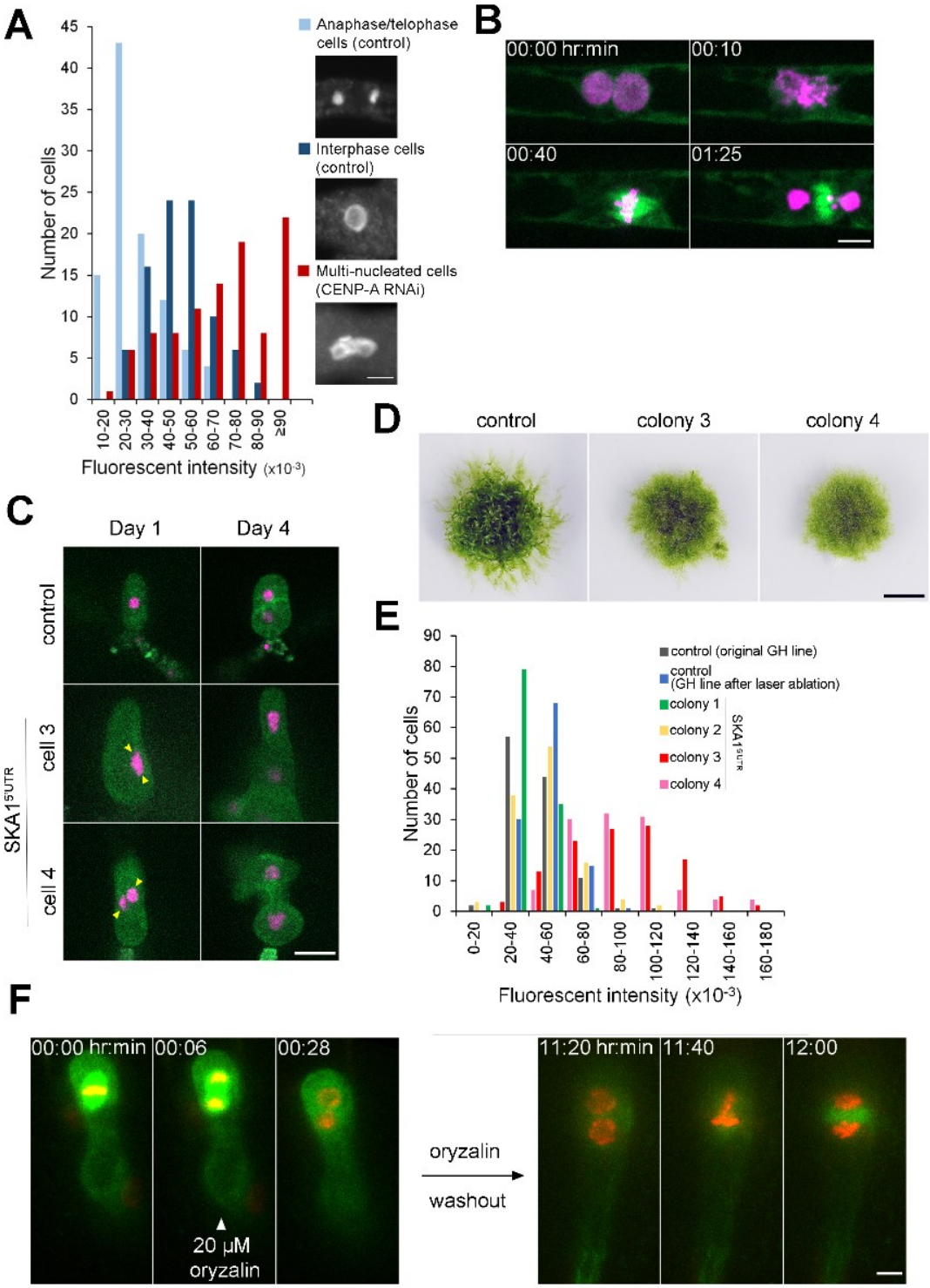

Figure 3. Cytokinesis failure in somatic cells can generate plants with whole-genome duplication
(A) Quantification of the nuclear DNA content. Anaphase/telophase cells were used as a standard for 1N nuclei (light blue). Interphase cells randomly selected in the control line mostly had double amounts of DNAs, as expected (dark blue), whereas cells that failed cytokinesis had higher ploidy (red). DNA amounts are shown as fluorescent intensity of the DAPI-stained nuclei per cell after subtraction of the cytoplasmic background. (B) Representative images of mitotic entry and single spindle formation of the multi-nucleated cell in the *P. patens* SKA1 RNAi line. Bar, 5 µm. (C) Regeneration of a single cell isolated by laser dissection microscopy from the control cell line (GH) or multi-nucleated cells from SKA1 RNAi line (multi-nuclei are marked with yellow arrowheads). Bar, 50 µm. (D) Moss colonies regenerated from single cells. Bar, 0.5 cm. (E) Quantification of the nuclear DNA content in the interphase nucleus of regenerated moss colonies, corresponding to (C) and (D). (F) *(Left)* Cytokinesis failure induced by oryzalin addition in the first division of the *A. thaliana* embryo. *(Right)* Cell division of the bi-nucleated embryonic cell following oryzalin washout. Bar, 10 µm.

Supplemental materials

Abbreviations
CCAN – Constitutive Centromere Associated Network
Cit – Citrine
CPC – Chromosome Passenger Complex
GFP – green fluorescent protein
HR – homologous recombination
mCh – mCherry
MTs - microtubules
NEBD – nuclear envelope breakdown
RNAi – RNA interference
SAC – spindle assembly checkpoint

Full names
BMF1 *(Bub1)* - BUB1/MAD3 family 1
BubR1 *(*BMF2*)* - BUB1-related protein 1 *(*BUB1/MAD3 family 2*)*
CENP-A *(cenH3)* – centromere protein A *(centromeric Histone 3)*
CENP-C – centromere protein C
CENP-O – centromere protein O
CENP-S *(FAAP16, MHF1)* – Centromere protein S *(Fanconi anemia-associated polypeptide of 16 kDa; FANCM-associated histone fold protein 1)*
CENP-X *(FAAP10, MHF2)* – Centromere protein X *(Fanconi anemia-associated polypeptide of 10 kDa; FANCM-associated histone fold protein 2)*
Dsn1 – dosage suppressor of Nnf1
KNL1 *(Spc7; Blinkin)* – kinetochore null 1 *(spindle pole body component 7; Bub-linking kinetochore protein)*
KNL2 *(MIS18BP1)* – kinetochore null 2 *(Mis18-binding protein 1)*
MAD2 - mitotic arrest deficient 2
Mis12 – minichromosome instability 12
Mps1 – serine/threonine-protein kinase MPS1 (monopolar spindle protein 1)
Ndc80 *(HEC1)* - nuclear division cycle protein 80 *(highly expressed in cancer 1)*
Nnf1*(PMF1)* - necessary for nuclear function 1 *(Polyamine-modulated factor 1)*
Nsl1 - Nnf1 synthetic lethal 1
Nuf2 - nuclear filament-containing protein 2
SKA1, 2, 3 – spindle and kinetochore associated protein 1, 2, 3
Spc24, 25 - spindle pole body component 24, 25
SUN1 – SUN domain-containing protein 1
Taf9 – TATA box binding protein (TBP)-associated factor 9

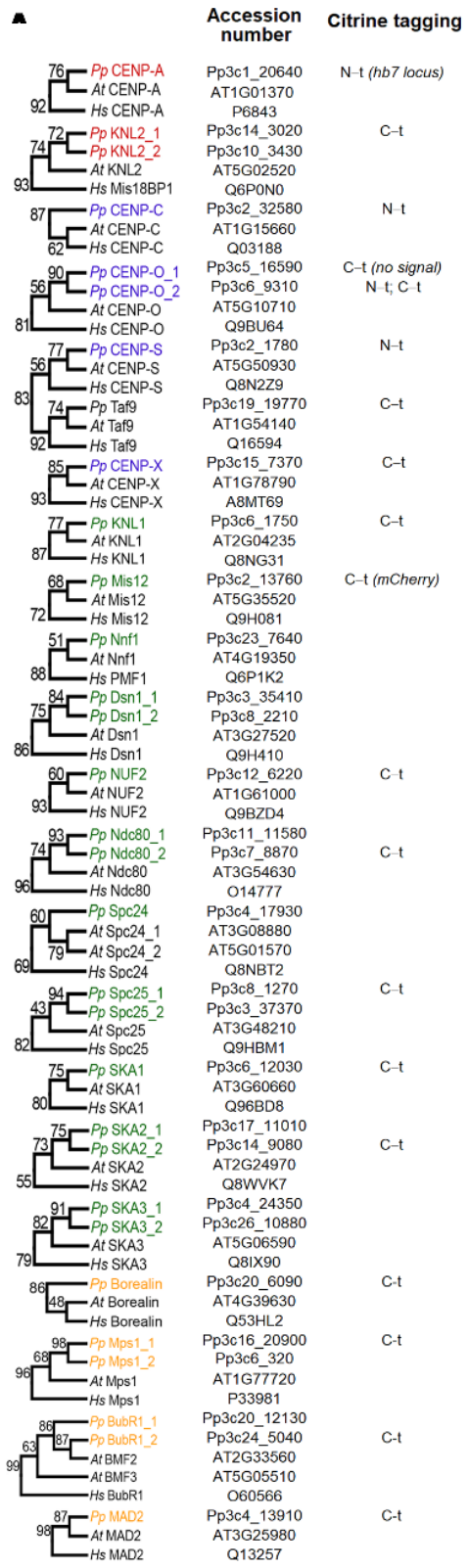

Figure S1. Summary of kinetochore protein tagging in *P. patens*

(left) Maximum-likelihood phylogenetic trees of conserved centromere/kinetochore proteins in *Physcomitrella patens*, *Arabidopsis thaliana* and *Homo sapiens*. Numbers represent bootstrapping values (above 50%) calculated from 1000 replications. *(right)* Summary of Citrine endogenous tagging experiments ("N-t" stands for N-terminal tagging; "C-t" stands for C-terminal tagging), pursued in this study. Accession numbers for each protein correspond to Phytozome (https://phytozome.jgi.doe.gov/) for *Physcomitrella patens*; TAIR (https://www.arabidopsis.org/) for *Arabidopsis thaliana* and UniProt (http://www.uniprot.org/) for *Homo sapiens*.

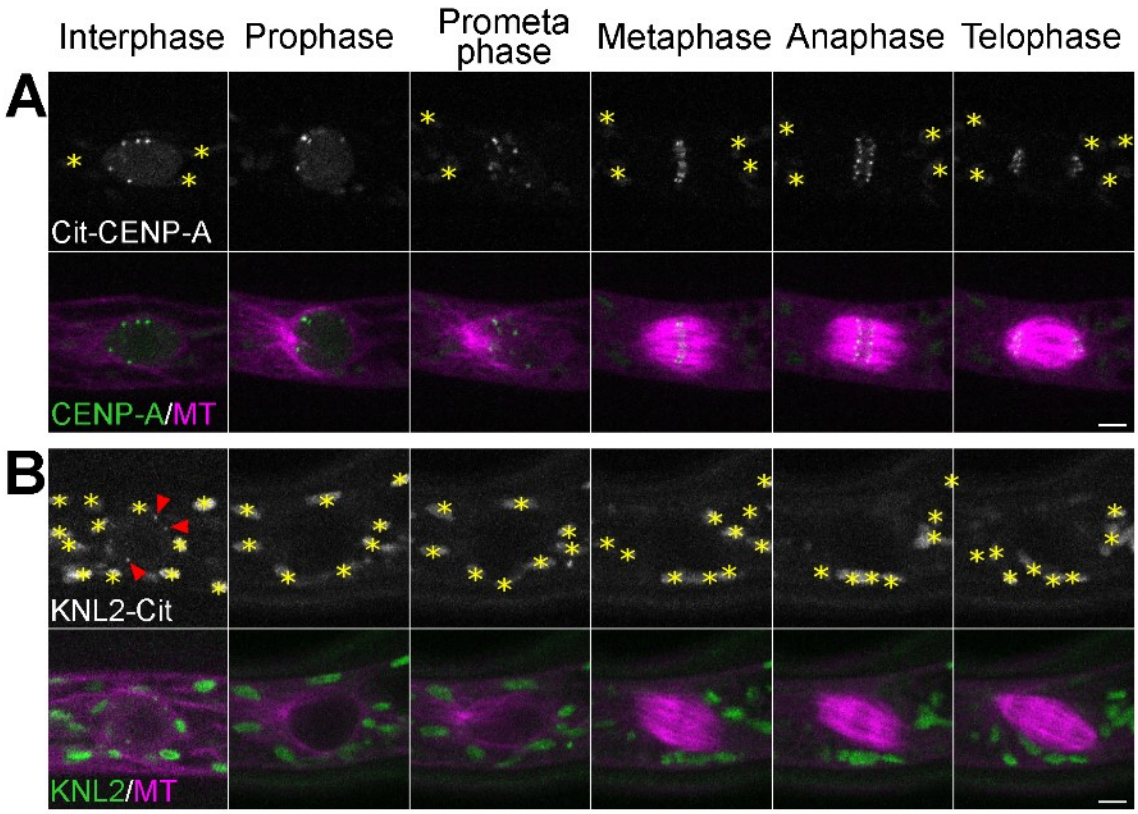

Figure S2. Localization of CENP-A and KNL2/MIS18BP1 during cell division
Live imaging of *P. patens* protonemal apical cells expressing mCherry-tubulin (magenta) and Citrine-CENP-A (A) or KNL2-Citrine (B). Citrine-CENP-A data is an expanded version of Fig. 1. Autofluorescent chloroplasts are marked with yellow asterisks. Images were obtained at a single focal plane. CENP-A was localized at the centromeric region throughout the cell cycle, whereas KNL2-Citrine was visible only during interphase (red arrowheads). Bars, 5 µm.

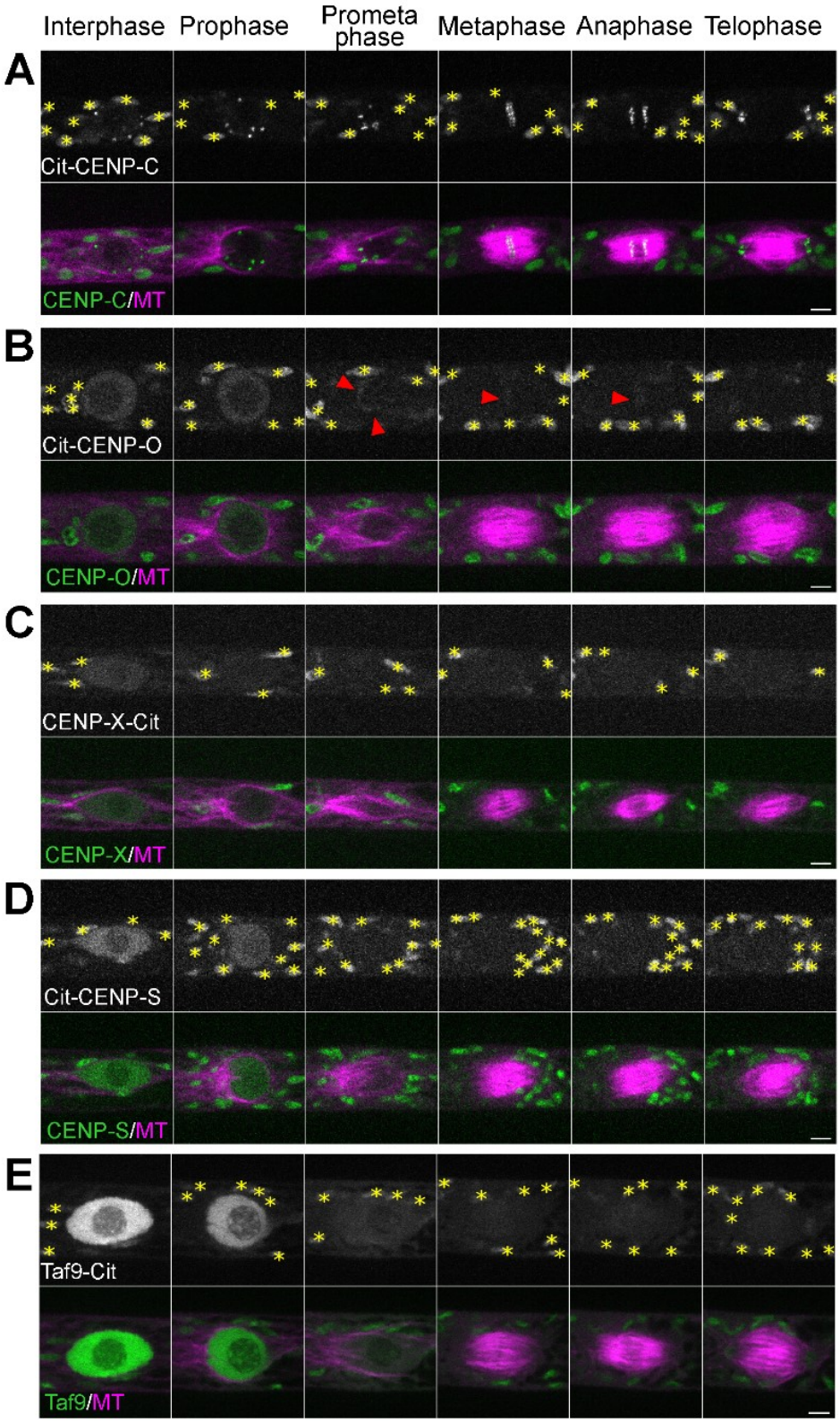

Figure S3. Localization of CCAN proteins during cell division

Live imaging of *P. patens* protonemal apical cells expressing mCherry-tubulin (magenta) and Citrine-tagged (green) CENP-C (A), CENP-O (B), CENP-X (C), CENP-S (D) and CENP-S-like protein Taf9 (E). Citrine-CENP-C and Citrine-CENP-S data are expanded versions of Fig. 1. Autofluorescent chloroplasts are marked with yellow asterisks. Images were obtained at a single focal plane. CENP-C was localized at the centromere from G2 to telophase, whereas none of the other CCAN proteins showed punctate signals throughout the cell cycle. CENP-O showed weak midzone localization from prometaphase to anaphase (arrowheads). Bars, 5 µm.

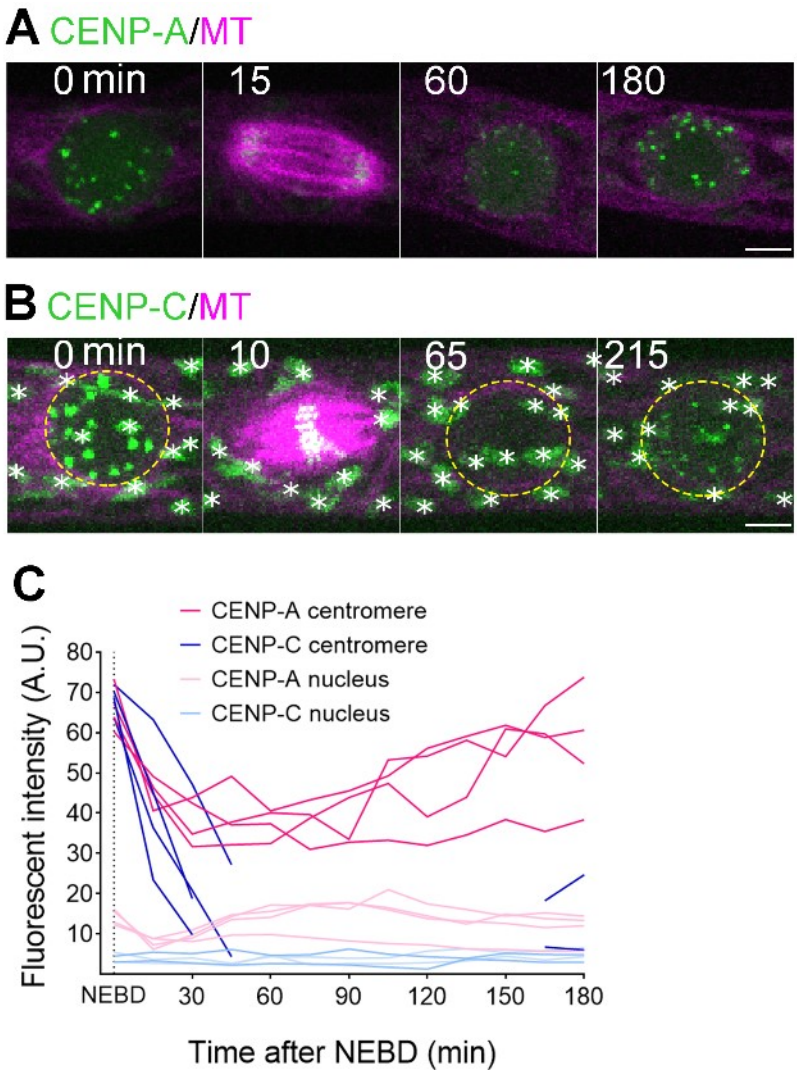

Figure S4. CENP-C is not a constitutive centromeric protein in *P. patens*
Citrine-CENP-A (A) and Citrine-CENP-C (B) localization starting from NEBD. At each time point, ten z-sections were acquired (separated by 1 µm). Merged images of mCherry-tubulin (single focal plane) and a maximum Z-projection of Citrine-CENP-A or -CENP-C are presented. Note that Citrine-CENP-C (B) brightness/contrast were enhanced to confirm no centromeric signals at 65 min. White stars label autofluorescent chloroplasts and yellow dotted lines mark the position of the nucleus. Bars, 5 µm. (C) Relative intensity plot of Citrine signals at the centromeres and at the non-centromeric region in the nucleus (background measurement). Each line represents average relative fluorescent intensity of ≥ 6 centromeres or ≥ 6 non-centromeric regions inside the nucleus in a single cell, measured every 15 min from the maximum Z-projection. Note that we could not identify centromeric Citrine-CENP-C signals during ~2 h after mitotic exit, and therefore, the data are missing from the graph.

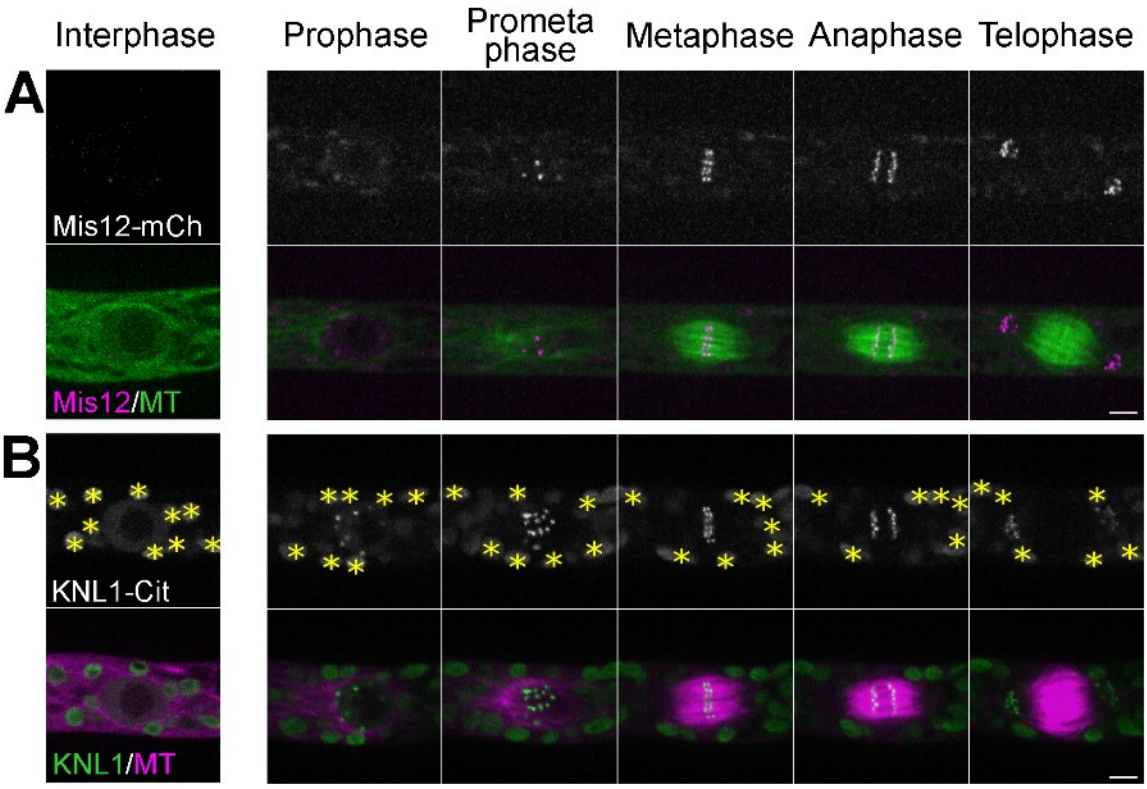

Figure S5. Localization of Mis12 and KNL1 during cell division
Live imaging of *P. patens* protonemal apical cells expressing GFP-tubulin and Mis12-mCherry (A) or mCherry-tubulin and KNL1-Citrine (B) KNL1-Citrine data is an expanded version of Fig. 1. Autofluorescent chloroplasts are marked with yellow asterisks. Images were acquired at a single focal plane. Bars, 5 µm.

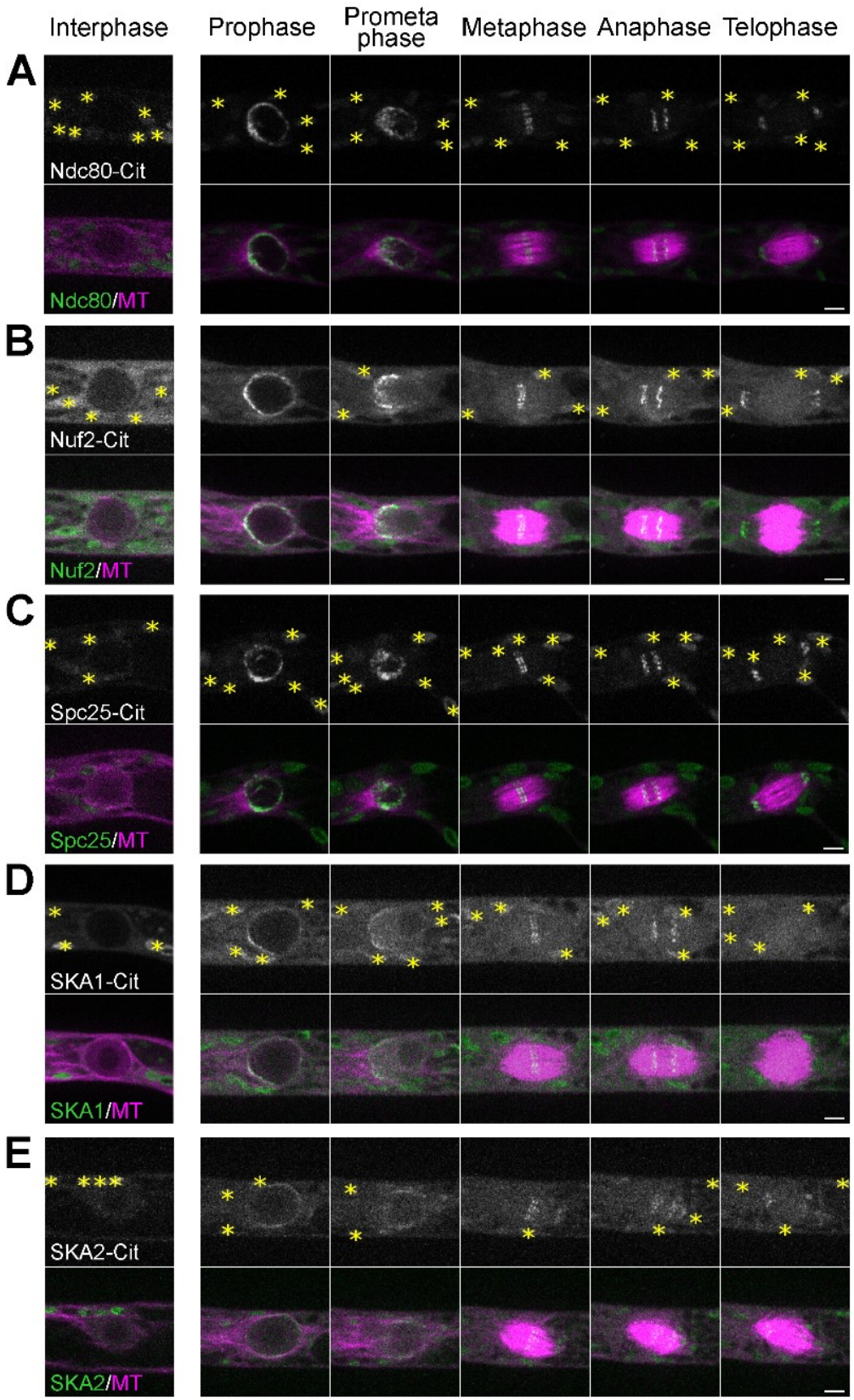

Figure S6. Localization of outer kinetochore proteins during cell division
Live imaging in *P. patens* protonemal apical cells expressing mCherry-tubulin (magenta) and Citrine-tagged (green) Ndc80 (A), Nuf2 (B), Spc25 (C), SKA1 (D) and SKA2 (E). Ndc80-Citrine and SKA1-Citrine data are expanded versions of Fig. 1. Autofluorescent chloroplasts are marked with yellow asterisks. Images were acquired at a single focal plane. Punctate Citrine signals appeared after prometaphase. Bars, 5 µm.

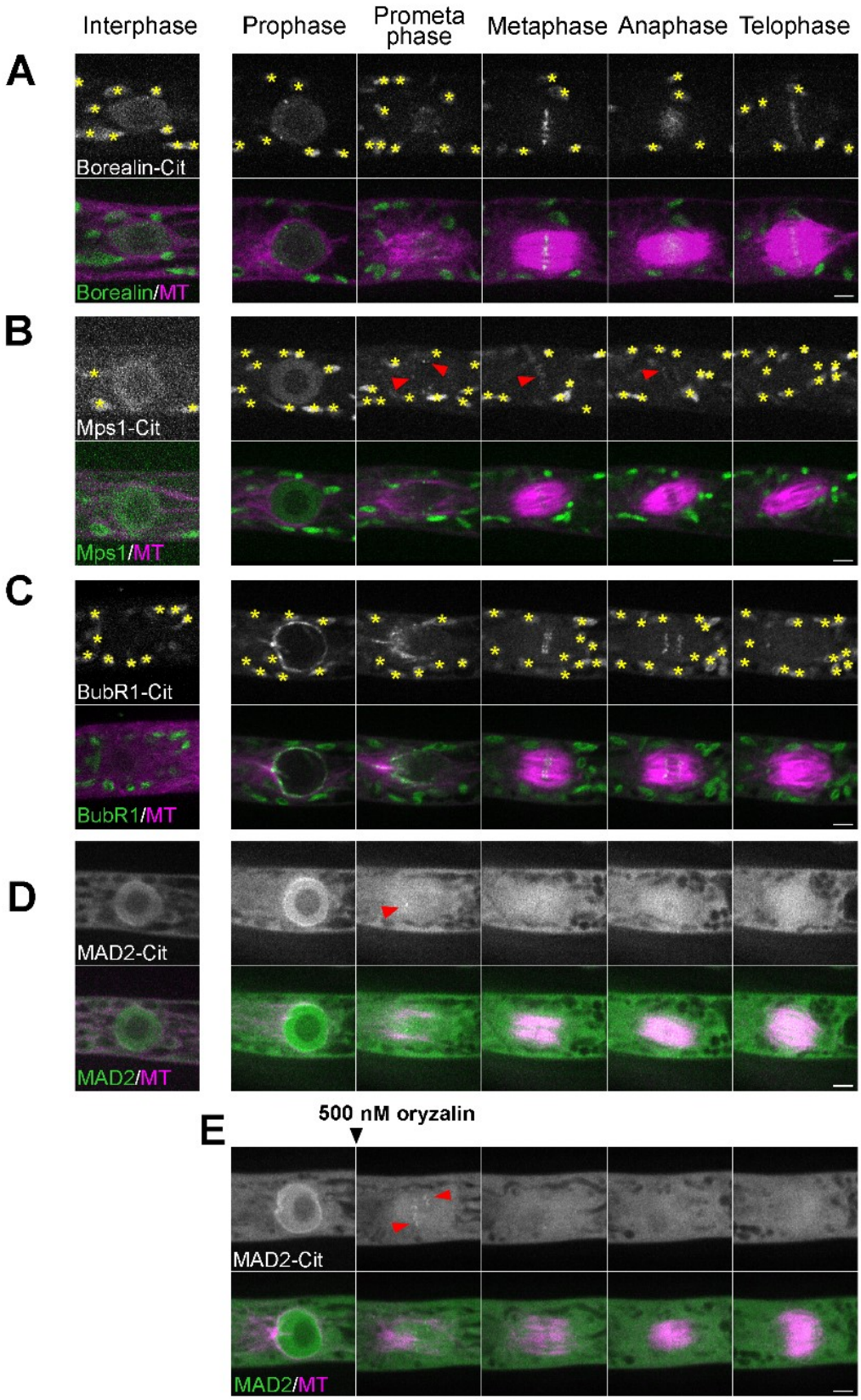

Figure S7. Localization of CPC and SAC proteins during cell division
Live imaging of *P. patens* protonemal apical cells expressing mCherry-tubulin (magenta) and Citrine-tagged (green) Borealin (A), Mps1 (B), BubR1(C) and Mad2 (D, E). Red arrowheads indicate punctate signals. Note that kinetochore localization of Mad2 was more clearly observed following addition of the microtubule-depolymerizing drug (500 nM oryzalin) (E). Autofluorescent chloroplasts were marked with yellow asterisks. Images were acquired at a single focal plane. Bars, 5 µm.

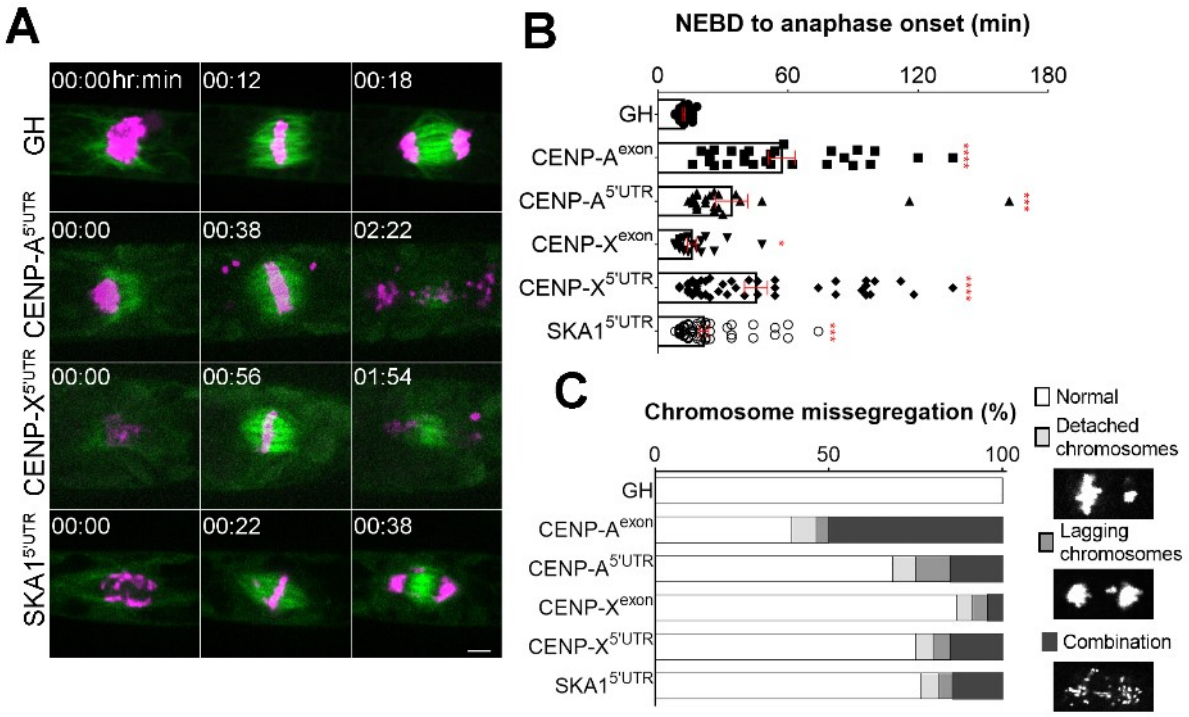

Figure S8. Chromosome segregation defects following depletion of CENP-A, CENP-X or SKA1
(A) Representative mitotic progression and chromosome missegregation caused by depletion of CENP-A, CENP-X or SKA1. "GH" is the control line. Bar, 5 µm. (B) Duration of mitosis (from NEBD to anaphase onset) was calculated from high-resolution live-cell imaging data for each RNAi line and the control line (GH). Bars indicate mean and SEM, whereas asterisks indicate significant differences compared with the control (*P < 0.04, ***P < 0.0007, ****P < 0.0001; two-tailed *t*-test). More than 20 cells were analyzed for each line. (C) Frequency of chromosome missegregation in different RNAi lines. Chromosome missegregation defects were classified into three types: chromosomes detached from the metaphase plate (detached chromosomes), lagging chromosomes in anaphase (lagging chromosomes), and their combination. More than 20 cells were analyzed for each line.

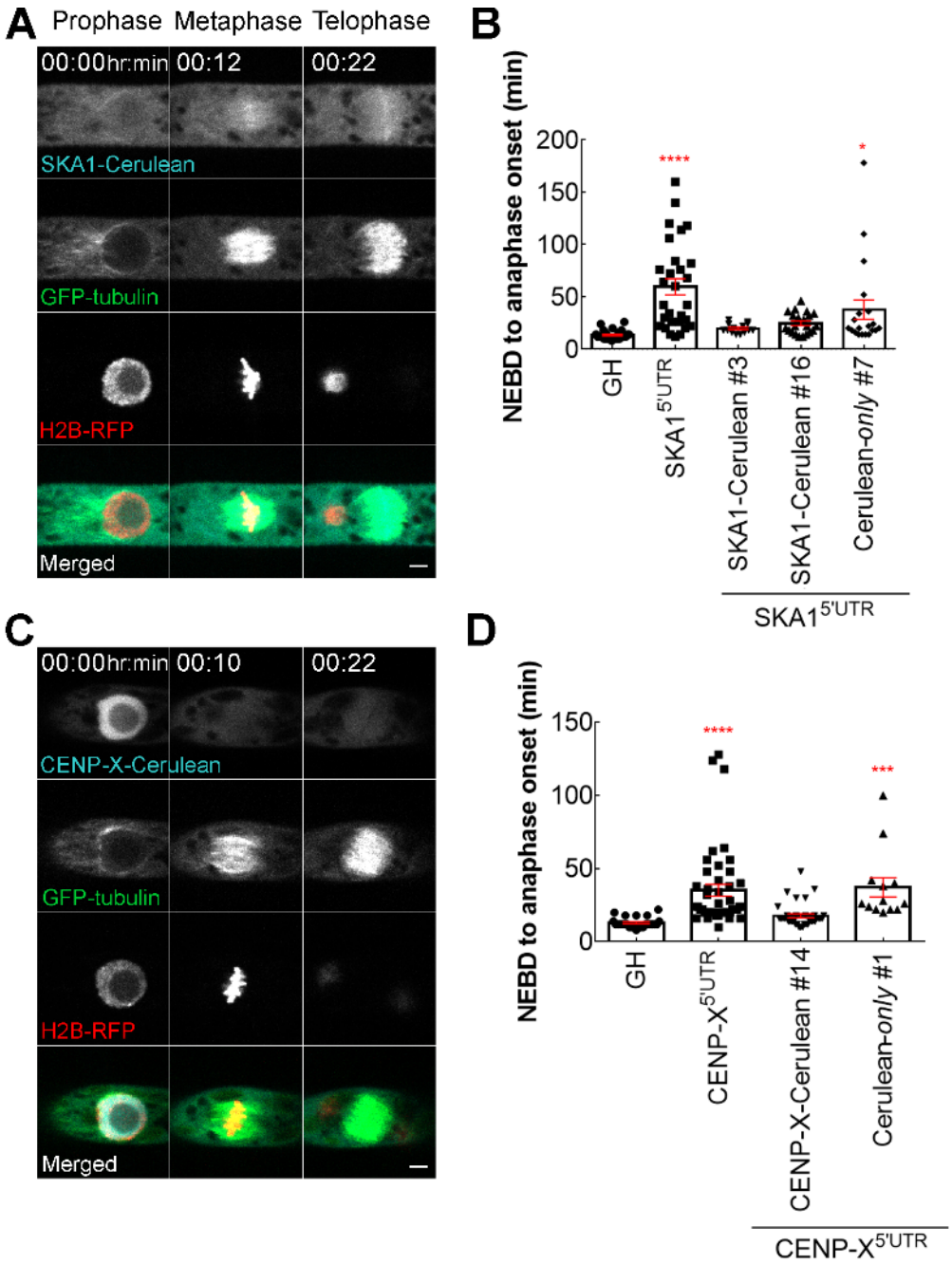

Fig. S9. Rescue of RNAi phenotypes by ectopic expression of SKA1-Cerulean or CENP-X-Cerulean
Live imaging of *P. patens* protonemal apical cells expressing SKA1-Cerulean (A) or CENP-X-Cerulean (C) in the SKA1 5'UTR RNAi or CENP-X 5'UTR RNAi lines, respectively. RNAi was induced by addition of β-estradiol to the culture medium at the final concentration of 5 µM, 5–6 days prior to observation. Bar, 5 µm. (B, D) Mitotic duration (from NEBD to anaphase onset) for each RNAi line with or without the rescue construct (two independent SKA1 rescue lines [#3, #16] were analyzed). "GH" is the mother line used for RNAi transformation. Bars indicate mean and SEM, whereas asterisks indicate significant differences (*P < 0.03, ***P < 0.001, ****P < 0.0001; one-way ANOVA). More than ten cells were analyzed for each line.

CENP-A^{exon}; CENP-A$^{5'UTR}$	Cytokinesis defect	Cytokinesis complete
Lagging chromosomes observed in the midzone for ≤ 4 min	0	8
Lagging chromosomes observed in the midzone for ≥ 12 min	9	0

CENP-X$^{5'UTR}$	Cytokinesis defect	Cytokinesis complete
Lagging chromosomes observed in the midzone for ≤ 4 min	0	4
Lagging chromosomes observed in the midzone for ≥ 8 min	14	0

SKA1$^{5'UTR}$	Cytokinesis defect	Cytokinesis complete
Lagging chromosomes observed in the midzone for ≤ 4 min	0	3
Lagging chromosomes observed in the midzone for ≥ 6 min	5	1

Table S1. Dataset used for Fisher's test in Fig. 2C

Movie S1. Localization of the centromere and CCAN proteins during cell division
Live-cell imaging was conducted in *P. patens* protonemal cells expressing mCherry-tubulin (magenta) and one of the following proteins tagged with Citrine(green): CENP-A, KNL2, CENP-C, CENP-O and CENP-S. Note that brightness/contrast of Citrine-CENP-O images have been enhanced. Images are single focal plane and were acquired every 30 s. Bar, 10 µm.

Movie S2. Transient disappearance of CENP-C from the kinetochore after cell division
Live-cell imaging was conducted in *P. patens* protonemal cells expressing mCherry-tubulin (magenta) and one of the following proteins tagged with Citrine(green): CENP-A, CENP-C and KNL2. Displayed are the the merged images of a single focal plane for mCherry-tubulin (magenta) and maximum-projection of the Z-stack for Citrine-tagged proteins. Images were acquired every 5 min. Bar, 10 µm.

Movie S3. Localization of the Mis12, KNL1, Nuf2 and SKA1 during cell division
Live-cell imaging was conducted in *P. patens* protonemal cells expressing mCherry-tubulin or GFP-tubulin (magenta) and one of the following proteins tagged with mCherry (for Mis12) or Citrine for KNL1, Nuf2 and SKA1. Images were acquired at a single focal plane every 30 s. Bar, 10 µm.

Movie S4. Chromosome missegregation after RNAi
Representative images of mitotic progression and chromosome missegregation caused by depletion of CENP-A or CENP-X or SKA1. RNAi was induced by addition of β-estradiol to the growth medium at final concentration of 5 µM, 5–6 days prior to observation. Images were acquired at a single focal plane every 2 min. Bar, 10 µm.

Movie S5. Cytokinesis defect associated with lagging chromosomes in anaphase
Representative images of correlation between lagging chromosomes and cytokinesis defect in CENP-A exon RNAi and SKA1 5'UTR RNAi lines. Note that minor lagging chromosomes observed in the midzone for ≤ 4 min did not affect cytokinesis (*upper rows*); however lagging chromosomes persistent for ≥ 6 min resulted in cytokinesis failure (*bottom rows*). This correlation is conserved in both CENP-A exon RNAi and SKA1 5'UTR RNAi lines. Cytokinesis failure was concluded when the nucleus moved without restraint of the cell plate. RNAi was induced by addition of β-estradiol to the growth medium at final concentration of 5 µM, 5–6 days prior to observation. Images were acquired at a single focal plane every 2 min. Bar, 10 µm.

Movie S6. Visualization of the cell plate formation using FM4-64 dye
Representative images of cytokinesis in the control GH line *(upper row)*, SKA1 5'UTR RNAi line with minor lagging chromosomes *(middle row),* and with persistent lagging chromosomes *(bottom row)*. Cell plate formation was visualized with 25 µM endocytic FM4-64 dye added during metaphase. FM4-64 dye was prone to photobleaching, and therefore was sometimes supplied multiple times during long-term imaging *(bottom row)*. Images were acquired at a single focal plane every 2 min. Bar, 10 µm.

Movie S7. Mitotic entry of the multi-nucleated cell in *P. patens*
SKA1 5'UTR RNAi was induced by addition of β-estradiol to the growth medium at final concentration of 5 µM, 5–6 days prior to observation. Multi-nucleated cells resulting from cytokinesis failure were monitored with the spinning-disk confocal microscope. Images were acquired at a single focal plane every 5 min. Bar, 10 µm.

Movie S8. Mitotic entry of the bi-nucleated cell following induced cytokinesis failure in *A. thaliana* embryo
(left) We induced cytokinesis failure by adding 20 µM oryzalin during the anaphase. Images were acquired every 2 min. *(right)* Mitotic entry of the bi-nucleated embryo following oryzalin washout (we did not acquire images during the washout step). Images were acquired every 10 min. Images are maximum Z-projection of five Z-planes separated by 5 µm. Bars, 10 µm.

Dataset S1. *Physcomitrella patens* transgenic lines generated in this study
Dataset S2. Plasmids and primers used in this study